On the role of domain aspect ratio in the westward intensification of wind-driven surface ocean circulation

Nathan Paldor[1], Kaushal Gianchandani[1], and Hezi Gildor[2]

[1]Hebrew University of Jerusalem
[2]The Hebrew University

November 23, 2022

Abstract

The two seminal studies on westward intensification, carried out by Stommel and Munk over 70 years ago, are revisited to elucidate the role of the domain aspect ratio (i.e.˜meridional to zonal extents of the basin) in determining the width and speed of a western boundary current (WBC). We examine the general mathematical properties of the two models by transforming them to differential problems that contain only two parameters — the domain aspect ratio and the non-dimensional damping (viscous) coefficient. Simple proxies of width and speed (and hence the transport that equals their product) of the WBC are derived from analytical solutions of the non-dimensional vorticity equations in the relevant region of the (damping, aspect ratio) parameter space. These analytically determined proxies are then benchmarked against numerical simulations of the corresponding time-dependent equations. In both models, the three proxies vary as a power law in the domain aspect ratio and in particular, the non-dimensional transport varies linearly with the domain aspect ratio.

On the role of domain aspect ratio in the westward intensification of wind-driven surface ocean circulation

Kaushal Gianchandani[1], Hezi Gildor[1], and Nathan Paldor[1]

[1]Fredy and Nadine Herrmann Institute of Earth Sciences, Hebrew University of Jerusalem, Jerusalem, Israel

Key Points:

- Two classical model's of wind-driven ocean circulation, Stommel (1948) and Munk (1950), are generalized in a manner that the spatial structure of the flow is explained by only two non-dimensional parameters — damping and the domain aspect ratio (the ratio of meridional to zonal extent of the basin).
- Proxies based only on the two non-dimensional parameters are proposed to estimate the width and speed (and consequently the transport) of the western boundary current, and their validity is benchmarked against numerical simulations.
- The dependence of the proxies on the domain aspect ratio is explicitly identified, in particular, the linear dependence of the non-dimensional transport on the aspect ratio is underscored.

Corresponding author: Nathan Paldor, `nathan.paldor@huji.ac.il`

Abstract

The two seminal studies on westward intensification, carried out by Stommel and Munk over 70 years ago, are revisited to elucidate the role of the domain aspect ratio (i.e. meridional to zonal extents of the basin) in determining the width and speed of a western boundary current (WBC). We examine the general mathematical properties of the two models by transforming them to differential problems that contain only two parameters — the domain aspect ratio and the non-dimensional damping (viscous) coefficient. Simple proxies of width and speed (and hence the transport that equals their product) of the WBC are derived from analytical solutions of the non-dimensional vorticity equations in the relevant region of the (damping, aspect ratio) parameter space. These analytically determined proxies are then benchmarked against numerical simulations of the corresponding time-dependent equations. In both models, the three proxies vary as a power law in the domain aspect ratio and in particular, the non-dimensional transport varies linearly with the domain aspect ratio.

1 Introduction

Perhaps the most striking characteristic of the surface circulation in an ocean basin is the east-west asymmetry: strong and narrow pole-ward currents often referred to as the "western boundary currents" (WBC) flow along the western boundary of the oceans while the return equator-ward flow is weak and wide. In the North Atlantic this current is the Gulf Stream, and it was known to oceanographers and explorers for a few centuries — see Stommel (1958) for a historical review. Similar WBCs exist in other basins as well and these include the Kuroshio in the North Pacific and the Brazil current in the South Atlantic. These currents transport large amount of heat from low to high latitudes, thus playing an important role in the climate system. The winds, though, are easterlies along the equator (the Trade winds) and westerlies around 40°N. There are no strong northward winds along the western boundaries of the ocean basins and, as is well understood now, the WBCs are not obviously correlated with the overlying wind patterns.

Henry Stommel, apparently in his first paper (Stommel, 1948, hereafter referred to as S48) as an oceanographer [see e.g. Kunzig (1999)] was the first to formulate a simple, yet comprehensive, mathematical model of the WBCs. S48 is now regarded as a seminal paper (e.g. http://empslocal.ex.ac.uk/people/staff/gv219/classics.d/oceanic.html) in theoretical physical oceanography. S48's model probably provided the simplest possible explanation for the existence of WBCs: in this linear and frictional model on the $\beta-$plane the ocean was taken to be a rectangular box with a flat bottom forced by a cos(latitude)-dependent zonal wind pattern. (Munk, 1950, hereafter referred to as M50) further extended this work to a different frictional (viscous) parameterization and a more general form of the wind stress.

In the last 70 years, both models have been modified and extended to further explore the phenomenon of westward intensification in different settings or to evaluate the importance of different specific processes and terms in the governing equations (Munk & Carrier, 1950; Veronis, 1966a, 1966b; Pedlosky, 2013; Vallis, 2017, and references therein).

As in S48 and M50, a large number of these subsequent studies employed the dimensional form of the governing equations which are the time-independent rotating linearized shallow water equations compounded by friction and forcing. These dimensional models include numerous parameters: the zonal and meridional extents of the basin; either the coefficient of linear drag (i.e. the coefficient in the Rayleigh frictional term) or the kinematic eddy viscosity (i.e. the coefficient in parameterization of the viscous term); the amplitude (and possibly meridional structure) of the wind stress; the gradient of Coriolis frequency ($\beta-$effect). Here we present an alternate, concise, formulation that can be employed to investigate the depth averaged wind-driven ocean circulation is a non-dimensional form of the equations and this formulation involves fewer (non-dimensional) parameters.

The aim of this study is to underscore the role of the domain aspect ratio (i.e. the ratio between the basin's meridional and zonal extents) in S48's and M50's models of westward intensification. In our non-dimensional formulation of the models, the domain aspect ratio is one of the two parameters that determines the solutions of the differential equations [while the other parameter is the non-dimensional frictional (viscous) coefficient]. A few of the previous studies that followed S48 and M50 [e.g. Pedlosky (2013); Vallis (2017)] have also employed the non-dimensional form of the equations but none of these addressed the effect of the domain aspect ratio on the solutions. For instance, in the most succinct model proposed by Vallis (2017) the number of non-dimensional parameters is reduced to one [i.e. the frictional (viscous) coefficient] but this model studies the dynamics of the flow in a square basin where the meridional and zonal extents are identical. Our approach yields explicit expressions for the proxies of the transport, width and speed of the WBC in terms of the two non-dimensional model parameters. The results demonstrate that all of these proxies depend sensitively on the domain aspect ratio.

The paper is organized as follows. Section 2 sketches the derivation of the two-parameter, non-dimensional, vorticity equations corresponding to S48's and M50's models and outlines the solution for the stream function ψ in the two cases. Explicit expressions for the width, speed and transport of the WBC are derived from these solutions for ψ. The applicability of these analytical expressions for relevant values of the model parameters is validated in Section 3 by simulating the time-dependent equations and we discuss the results and conclude in Section 4.

2 The two-parameter differential problems, their solutions and associated proxies

2.1 S48's non-dimensional counterpart

We begin by scaling S48's dimensional vorticity equation for the spatial structure of the stream function as follows: x (the zonal coordinate) on L_x; y (the meridional coordinate) on L_y and ψ (the stream function) on $\gamma \beta L_y^3$ where L_x and L_y are the zonal and meridional dimensions of the barotropic ocean, respectively, β is the meridional gradient of the Coriolis frequency and $\gamma = \tau_0 \left(\frac{\pi}{\rho_0 H_0 \beta L_y^2} \right) \left(\frac{L_x}{\beta L_y^2} \right)$ is the non-dimensional amplitude of the wind stress, τ_0, with H_0 — the depth of the basin and ρ_0 — water density in the barotropic ocean. With this scaling the non-dimensional form of S48's vorticity equation is:

$$\alpha \nabla^2 \psi + \frac{\partial \psi}{\partial x} = \sin(\pi y) \tag{1}$$

$$\alpha = r \left(\frac{L_x}{\beta L_y^2} \right), \qquad \nabla^2 = \delta^2 \frac{\partial^2}{\partial x^2} + \frac{\partial^2}{\partial y^2}. \tag{2}$$

Here ∇^2 is the Laplacian, $\delta = \frac{L_y}{L_x}$ is the ratio of meridional and zonal extents of the basin (refereed to as the domain aspect ratio) and α is the non-dimensional parameter (referred to as the damping) proportional to r — the Rayleigh friction coefficient. Variants of (1) appear in many textbooks e.g. Vallis (2017). It is evident from (1) and (2) that the two parameters, α and δ, govern the structure of the flow in the basin. The no normal flow conditions at the basin's boundaries mandate that the stream function ψ satisfies the boundary conditions: $\psi(x,0) = \psi(1,y) = \psi(x,1) = \psi(0,y) = 0$.

It should be stressed that due to the different scaling employed in the two works, α in (1) differs from the same coefficient that appears in S48's dimensional equation: in the present study the boundary conditions are imposed at $x = 0; 1$ and $y = 0; 1$ whereas in S48's study the basin's width and length appear separately in the boundary conditions in addition to α (that appears in the differential equation itself).

Our particular choice of scaling enables us to lump the five dimensional parameters in S48's model — zonal and meridional extent of the basin, gradient of Coriolis frequency,

wind stress amplitude and Rayleigh friction coefficient — into just two non-dimensional ones: α and δ (that appears in the first term of the Laplacian). The two-parameter vorticity equation, (1), succinctly brings out some general and salient features of the depth averaged wind-driven circulation in a rectangular basin which will be highlighted below.

For sufficiently smooth solutions the flow in the interior of the basin is expected to be frictionless in which case $\alpha\nabla^2\psi$ can be neglected there and the vorticity equation, (1), reduces to $\frac{\partial\psi}{\partial x} = \sin(\pi y)$ i.e. the equivalent of Sverdrup balance (Sverdrup, 1947). On the other hand, neglecting the planetary vorticity gradient term $\left(\frac{\partial\psi}{\partial x}\right)$ yields the dominant balance in a non-rotating basin in which case the vorticity equation (1) reduces to $\alpha\nabla^2\psi = \sin(\pi y)$, i.e. Poisson's equation that can be solved using conventional techniques.

The interplay between the three terms in the inhomogeneous partial differential vorticity equation, (1), can be easily interpreted by repeating the procedure employed in S48 to obtain the general form of solutions of (1). An explicit expression for the solution ψ is given by

$$\psi(x, y) = \frac{1}{\alpha\pi^2} \sin(\pi y)(pe^{Ax} + qe^{Bx} - 1) \tag{3}$$

where

$$
\begin{aligned}
p &= \frac{1 - e^B}{e^A - e^B} \\
q &= 1 - p
\end{aligned}
$$

and

$$
\begin{aligned}
A &= -\frac{1}{2\alpha\delta^2} + \frac{\pi}{\delta}\sqrt{1 + \frac{1}{4\pi^2\alpha^2\delta^2}}, \\
B &= -\frac{1}{2\alpha\delta^2} - \frac{\pi}{\delta}\sqrt{1 + \frac{1}{4\pi^2\alpha^2\delta^2}}.
\end{aligned}
$$

The corresponding explicit expressions for u and v are:

$$
u(x, y) = \frac{\partial\psi}{\partial y} = \frac{1}{\alpha\pi}\cos(\pi y)(pe^{Ax} + qe^{Bx} - 1) \tag{4}
$$

$$
v(x, y) = -\delta\frac{\partial\psi}{\partial x} = -\frac{\delta}{\alpha\pi^2}\sin(\pi y)(pAe^{Ax} + qBe^{Bx}) \tag{5}
$$

For completeness, we list in the Supporting Information some typos in S48's expressions for u and h (but not ψ itself). With the scaling adopted in the present study the dimensional counterparts of u and v (denoted by u^* and v^*, respectively) are: $u^* = u\gamma\beta L_y^2$ and $v^* = v\gamma\beta L_y^2$.

2.1.1 Analytic approximations in limiting cases for S48's model

For a given value of δ, the spatial distribution of the streamlines in the basin is determined by the value of α, the only other free parameter in (1). Figure 1(a),(c) depicts the stream function for two α-regimes of S48:

(i) $\alpha \leq O(1)$ (i.e. weak damping)
(ii) $\alpha > O(1)$ (i.e. strong damping).

In these two regimes of α the complicated expressions in (3), (4) and (5) can be greatly reduced as is shown below.

For $\alpha \leq O(1)$, the solution of ψ in (3) becomes linear in x and thus can satisfy only one boundary condition out of two. This solution is commonly assumed to approximate the
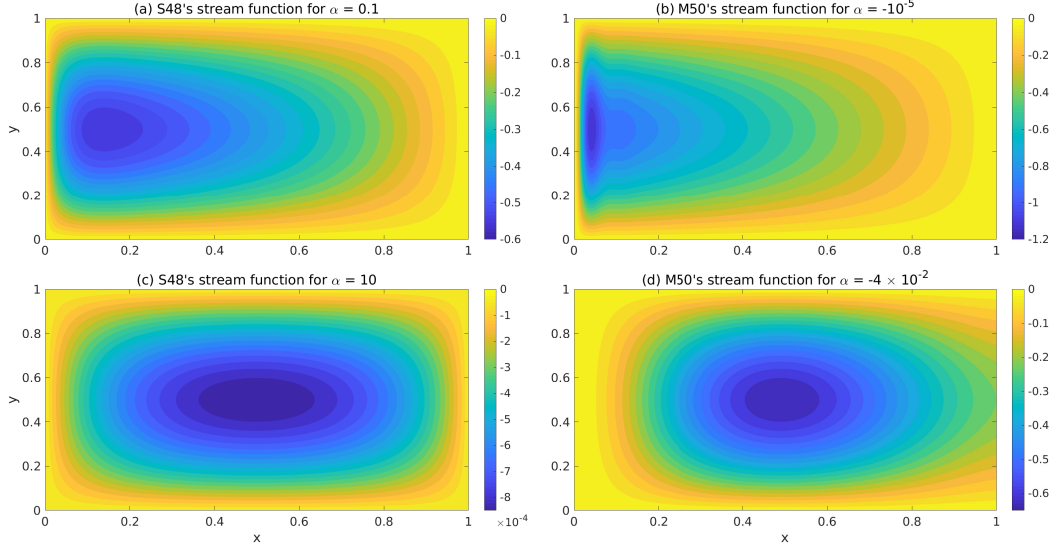
Figure 1. The stream functions in different regimes of the α parameter-space in the two models for $\delta = 2\pi/10$: (a),(b) weak damping [$\alpha \leq O(1)$ in S48's model and $|\alpha| \leq O(10^{-3})$ in M50's model] — there exists a narrow fast flowing current along the western edge of the basin; (c),(d) strong damping [$\alpha > O(1)$ in S48's model and $|\alpha| > O(10^{-3})$ in M50's model] — the stream function is (nearly) symmetric about $x = 0.5$ which indicates that there is no westward intensification.

exact solution for ψ in the frictionless interior of the basin while a different approximation applies in the narrow, frictional, boundary layer adjacent to $x = 0$. Figure 1(a) depicts this narrow boundary layer for $\alpha = 0.1$ where the stream function first decreases fast with x at small x and then increases slowly with x for large x. In the range of $\alpha \geq O(1)$, the solution ψ is symmetric about $x = \frac{1}{2}$ and can satisfy the two boundary conditions, $\psi(0, y) = 0\psi(1, y)$. This is demonstrated in the symmetric stream function depicted in Figure 1(c) for $\alpha = 10$. The explicit expressions of ψ in the two ranges of α are given in the Supporting Information.

From the expression given by (3) [and the two examples of ψ shown in Figure 1(a),(c)] one can infer that the width of the boundary layer depends on α, but the details of this dependence are not obvious since the coefficient A in equation (3) also depends on α. To determine the details of the dependence, we integrate the vorticity equation (1) w.r.t. x from $x = 0$ (i.e. the western boundary) to $x = \epsilon_{bc}$, where $\epsilon_{bc} \ll 1$ is the width of the WBC defined as the smallest value of x where $\frac{u}{v}$ is not small (i.e. the magnitude of u is similar to that of v). We further assume that inside the boundary layer, (i) $u \ll v$, so the Laplacian term can be approximated by $\nabla^2\psi \approx -\delta\frac{\partial v}{\partial x}$ and (ii) the meridional speed at $x = \epsilon_{bc}$ is negligible compared to its value at $x = 0$ i.e. $v(\epsilon_{bc}, y) \ll v(0, y)$. With these assumptions the integration of (1) yields the following simple expression for ϵ_{bc}:

$$\epsilon_{bc}(y) = \alpha\delta\frac{1}{\left(\frac{1}{v(0,y)} + \frac{1}{\delta}\right)} \approx \alpha\delta^2, \tag{6}$$

The second equality that makes ϵ_{bc} independent of y holds provided $v^* \sim 2 \text{ m s}^{-1}$ which for $\gamma \sim 5 \times 10^{-5}$ and $L_y \sim 6000$ km translates to $\frac{1}{v(0,y)} \sim 10^{-2}$ which is negligible compared to $\frac{1}{\delta} > 1$ (for $L_x \sim 10000$ km). For realistic parameter values where this estimate of ϵ_{bc} holds, it is linear with both α and δ^2. For typical values of α of 0.02, and for the above values of L_y and L_x, the width of the boundary layer is $\epsilon_{bc} \sim 0.007$ i.e. about 70 km.

163   To quantify the speed of the WBC we propose another proxy — the maximum speed
164 of the WBC i.e. $v_{bc} = v\left(0, \frac{1}{2}\right)$ [it can be easily verified that v_{bc} attains its maximal value
165 at $(x = 0, y = 1/2)$]. The expression for v_{bc}, obtained by substituting $x = 0$ and $y = 1/2$ in
166 (5), is given by:

$$v_{bc} = -\frac{\delta}{\alpha\pi^2}(pA + qB). \tag{7}$$

167   Following this expression, the corresponding dimensional maximal speed of the WBC
168 is given by: $v_{bc}^* = v_{bc}\gamma\beta L_y^2$. Numerical computation show that the term $pA + qB$ decreases
169 with α hence (7) implies that $v_{bc} \propto \frac{1}{\alpha^n}$ where $n > 1$ (see also Section 3 below).

170   Having identified proxies for the width and maximal speed of the current we are now
171 in position to formulate an expression for the transport of the WBC. The non-dimensional
172 transport, Tr, is given as $Tr = \epsilon_{bc}\left(\frac{1}{2}\right)v\left(0, \frac{1}{2}\right)$ which, under the assumption $\frac{1}{v\left(0,\frac{1}{2}\right)}, \ll \frac{1}{\delta}$
173 simplifies to:

$$Tr \approx \alpha\delta^2 v\left(0, \frac{1}{2}\right) = -\frac{\delta^3}{\pi^2}(pA + qB) \tag{8}$$

174   The dimensional depth integrated transport is given by $Tr^* = Tr \times \gamma H_0 L_x \beta L_y^2$.

2.2   M50's non-dimensional counterpart

176   The non-dimensional counterpart of M50's vorticity equation, obtained by employing
177 the scaling proposed in this study, is given by:

$$\alpha\nabla^4\psi + \frac{\partial\psi}{\partial x} = \sin(\pi y) \tag{9}$$

178 where $\alpha = -\mu\frac{L_x}{\beta L_y^4}$ is the damping, μ ($\sim 10^4$ m^2 s^{-1}) is the (dimensional) horizontal eddy
179 viscosity and $\nabla^4 = \delta^4\frac{\partial^4}{\partial x^4} + 2\delta^2\frac{\partial^4}{\partial x^2 \partial y^2} + \frac{\partial}{\partial y^4}$. We note that contrary to (2), α here is
180 negative. This dissimilarity arises because, unlike the parametrization in S48, in M50's
181 model the damping is parametrized by a biharmonic function. Also, in addition to stream
182 function vanishing at the edges of the basin, another set of boundary condition needs to be
183 specified in order to solve the 4th order equation (9) — there should be no flow tangential to
184 the basin's edges i.e. $\left.\frac{\partial\psi}{\partial x}\right|_{x=0,1} = \left.\frac{\partial\psi}{\partial y}\right|_{y=0,1} = 0$. Following the mathematical steps in Munk's
185 original paper yields the following solution of (9):

$$\psi = -\sin(\pi y)\left(1 - x + \frac{1}{\lambda}e^{\lambda(x-1)} - e^{-\lambda(x/2)}\left[\cos\left(\frac{\sqrt{3}\lambda x}{2}\right) + \frac{1 - 2/\lambda}{\sqrt{3}}\sin\left(\frac{\sqrt{3}\lambda x}{2}\right)\right]\right) \tag{10}$$

186 where $\lambda = \left(\frac{1}{-\alpha\delta^4}\right)^{1/3}$.

2.2.1   *Analytic approximations in limiting cases for M50's model*

188   Figure 1(b),(d) depicts the stream function for small and large damping in M50's model.
189 For large damping the stream function shown in Figure 1(d) is not entirely symmetric about
190 $x = \frac{1}{2}$. Also, unlike the behavior of the stream function in S48's model, the stream function
191 in M50's model skews more towards the eastern boundary with the increase in damping.
192 This, less than optimal, behavior of the stream function in M50's model occurs because the
193 stream function does not vanish identically along the eastern boundary and is, instead, a
194 function of α itself.

195   We now proceed to obtain the proxies for the width, speed and transport for M50's
196 non-dimensional counterpart. Integrating the vorticity equation to obtain the width of the
197 WBC (as was done for S48's non-dimensional counterpart in the previous sub-section) is
198 not an effective method because it yields a much too complicated algebraic equation in ϵ_{bc}.

Thus, for the non-dimensional equivalent of M50's model we propose that the width of the WBC is defined as the smallest value of $x > 0$ where $v(x, y = \frac{1}{2})$ vanishes. The velocity of the WBC corresponding to this model is given by:

$$v(x,y) = -\delta \frac{\partial \psi^w}{\partial x}. \tag{11}$$

Here ψ^w is the stream function close to the western boundary of the basin. The value of x closest to 0 at which $v\left(x, y = \frac{1}{2}\right)$ vanishes [determined by substituting $y = 1/2$ in (11) and finding the root using Mathematica] is:

$$\epsilon_{bc} = \frac{2}{\sqrt{3}\lambda} \cos^{-1}\left(-\frac{2\lambda - 1}{4\lambda^2 - 4\lambda - 4}\right) \approx \frac{\pi}{\sqrt{3}}(-\alpha)^{\frac{1}{3}} \delta^{\frac{4}{3}} \tag{12}$$

The approximation in (12) holds for $\lambda \gg 1$ which is satisfied for typical values of dimensional parameters that correspond to $\lambda > O(50)$. The dependence of the width of WBC on δ in both (6) and (12) highlights the importance of the domain aspect ratio in the dynamics of westward intensification.

We now propose that in M50's model a proxy of the speed of the WBC is the average speed of the current between $x = 0$ and $x = \epsilon_{bc}$ at $y = \frac{1}{2}$. Using (11), it is straightforward to determine:

$$v_{bc} = \frac{1}{\epsilon} \int_0^\epsilon v\left(x, \frac{1}{2}\right) \, dx = \frac{\delta}{\epsilon} \psi^w\left(x = \epsilon, y = \frac{1}{2}\right) \approx \frac{2}{5}(-\alpha\delta)^{-\frac{1}{3}} + \delta \tag{13}$$

Under the same assumption, the non-dimensional transport in the boundary current as calculated from $Tr = \epsilon_{bc} v_{bc}$ is given by:

$$Tr = \epsilon_{bc} v_{bc} = \delta\left(\frac{3}{4} + 2(-\alpha\delta^4)^{\frac{1}{3}}\right) \approx \frac{3}{4}\delta + O(\delta^2) \tag{14}$$

Surprisingly, in both S48's and M50's models the calculated transports of the WBCs are nearly independent of α – the dissipation parameter. This is due to the opposing power law α-dependencies of the width of the WBC and the typical meridional velocity in it. In the next section we numerically validate these analytical results.

3 Numerical validation

The proxies, ϵ_{bc}, v_{bc} and Tr, obtained in the previous section are validated here in two ways — (i) by comparing them with the numerical calculations of the exact expressions and (ii) by benchmarking these proxies against diagnostics that we propose to quantify the width and speed calculated from numerical simulations of the corresponding time-dependent equations.

3.1 Exact expressions versus approximations for the proxies

Figure 2(a),(b) depict the proxies: ϵ_{bc}, v_{bc} and Tr as a function of α in the two models: the circles denote the values given by the exact expressions and the solid lines — the corresponding approximate expressions derived above. In both models, the width of the WBC increases and its speed decreases with a (near) power law dependence on damping the (α for S48's model and $|\alpha|$ for M50's model). As is apparent from Figure 2(a),(b), the power law dependence of both the width and the speed of the WBC on α is valid for over two decades in both the models. In S48's model, however, the value of ϵ_{bc} shown in Figure 2(a) is not accurate for $\alpha > O(1)$ because the expression for ϵ_{bc} in (6) is not valid in this regime since the approximation $\frac{1}{v(0,y)} \ll \frac{1}{\delta}$ does not apply there. Thus, we conclude that the effect of α
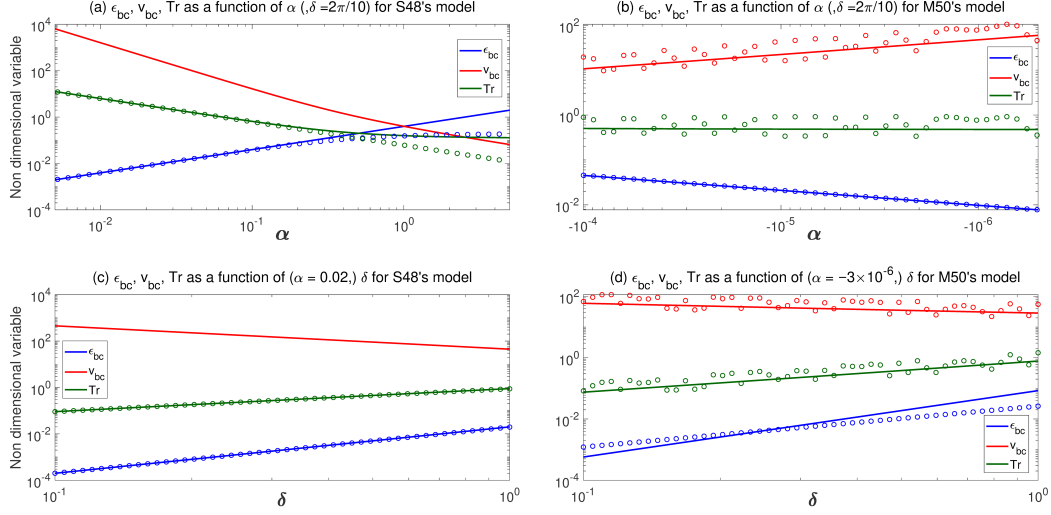
Figure 2. Non-dimensional width (ϵ_{bc}), speed (v_{bc}) and transport (Tr) of the WBC as a function of α and δ in the two models, in panels (a),(b) the domain aspect ratio is set to $\delta = 2\pi/10$ and in panels (c),(d) the damping is set to $\alpha = 0.02$ for S48's model and $\alpha = -3 \times 10^{-6}$ for M50's model. Circles show the exact value of the proxy and the solid line is the approximation. The 'exact value circles' are not plotted for v_{bc} in S48's model because no approximation is made to calculate the proxy v_{bc} in S48's model.

on the spatial structure of ψ (and hence on the width of the WBC) is limited to $\alpha < O(1)$ in S48's model. Unlike S48's model, α affects the spatial structure of the flow in M50's model over a wider range because $\psi(x = 0)$ varies with α [while in S48 $\psi(x = 0) = 0$]. The limitation on the validity of equation (6) is also reflected in the slight change of the slope of the v_{bc} (red) curve in Figure 2(a).

In M50's model the exact value of v_{bc} oscillates with α, however, the overall increase in v_{bc} with a decrease in damping ($|\alpha|$) is clearly evident and the approximate expression accurately captures the trend. As for the curve of the transport in M50 – it changes in a similar pattern to that of S48 as both shows negligible variation with α. The oscillations in the exact values of v_{bc} and consequently the Tr in M50's model arise because of the combination of cos and sin terms in ψ which have a significant contribution close to the western edge of the basin.

Up to this point our analysis focused on the way that α affects the dynamics in the two models and we now turn to the effect of the other non-dimensional parameter — δ. Determining analytically the dependence of v_{bc} and consequently of Tr on δ in S48's model is not straightforward because of the complicated dependence of $(pA + qB)$ in (3) on δ. Nevertheless, Figure 2(c) shows that ϵ_{bc}, v_{bc} and Tr vary as a power law in δ with exponents approximated by 2, −1 and 1 respectively, and that the differences between the exact and the approximate curves are negligible.

In contrast to S48's model, the (approximate) dependence of ϵ_{bc}, v_{bc} and Tr on δ in M50's model is straightforward [refer to (12), (13) and (14)]. Figure 2(d) depicts the aforementioned proxies as a function of δ. Each proxy follows a power law in δ and the exponents for ϵ_{bc}, v_{bc} and Tr are given by $\frac{4}{3}$, $\sim -\frac{1}{3}$ and ~ 1 respectively. The second terms in the expressions of v_{bc} and Tr in (13) and (14) are small corrections and do not affect significantly the exponents of the proxies. There are slight deviations between the exact and the approximate curves of ϵ_{bc} as a function of δ. Additionally, the approximations for
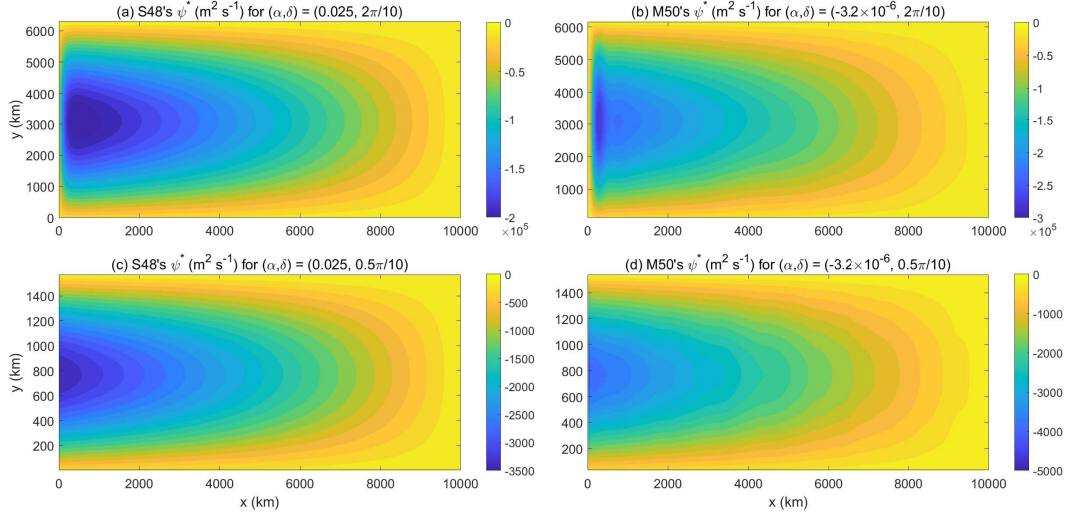
Figure 3. Dimensional stream functions (a) for S48's model — $(\alpha, \delta) = (0.025, 2\pi/10)$ and (b) for M50's model — $(\alpha, \delta) = (-3 \times 10^{-6}, 2\pi/10)$; panels (c),(d) are same as (a),(b) but for $\delta = 0.5\pi/10$. Note that the meridional extent of the basin in (c),(d) is one-fourth of that in (a),(b).

v_{bc} and Tr accurately capture the overall trends of the exact curves (but not the highly oscillatory behavior that arises from the sensitivity of these variables to the calculation of the various terms in the boundary layer).

3.2 Numerical simulations

The numerical simulations described below were carried out using the time-dependent shallow water equation (SWE) dimensional solver (Gildor et al., 2016; Shamir et al., 2019). This solver employs the finite difference method to solve SWEs on the $\beta-$plane. The simulations are carried out on an Arakawa C grid and the time differencing follows a leapfrog scheme. Though the solver can include nonlinear terms, for the purpose of this study, nonlinear terms were neglected. The reader should refer to Gildor et al. (2016) and Shamir et al. (2019) for a more detailed description of the solver.

The simulations presented in the present study were carried out using a barotropic ocean with the same characteristics as in S48 i.e. on an equatorial $\beta-$plane (i.e. $f_0 = 0$), forced by a wind stress which varies as $-\tau_0 \cos(\pi y/L_y)$ (where τ_0 is the amplitude of the wind stress and y and L_y denote the same dimensional quantities as in the preceding sections). Two of the dimensional parameters remained fixed in all the simulations presented below — the value of the gradient of Coriolis frequency (given by $\beta = 2 \times 10^{-11}$ m^{-1} s^{-1}) and the zonal extent of the basin given by ($L_x = 10000$ km). The other three dimensional parameters in the two WBC models i.e. the damping coefficients [Rayleigh friction coefficient (r) in S48's model and horizontal eddy viscosity (μ) in M50's model], the maximum amplitude of the prescribed forcing (τ_0), and the meridional extent of the basin (L_y) are varied such that α and γ remain constant and the effect of δ can be examined. The boundary conditions are: u^* = 0 along the basin's meridional boundaries and $v^* = 0$ along the basin's zonal boundaries. The numerical solver is integrated until a steady state is reached. The steady state of the time-dependent simulations is defined as the state at which the dependent variables in the SWEs (u^*, v^* and η^*) do not evolve any further for a sufficiently long time.

Figure 3(a),(c) depicts the dimensional stream function (ψ^*) in a steady state obtained by specifying the dimensional parameters as in S48's model (and the corresponding values
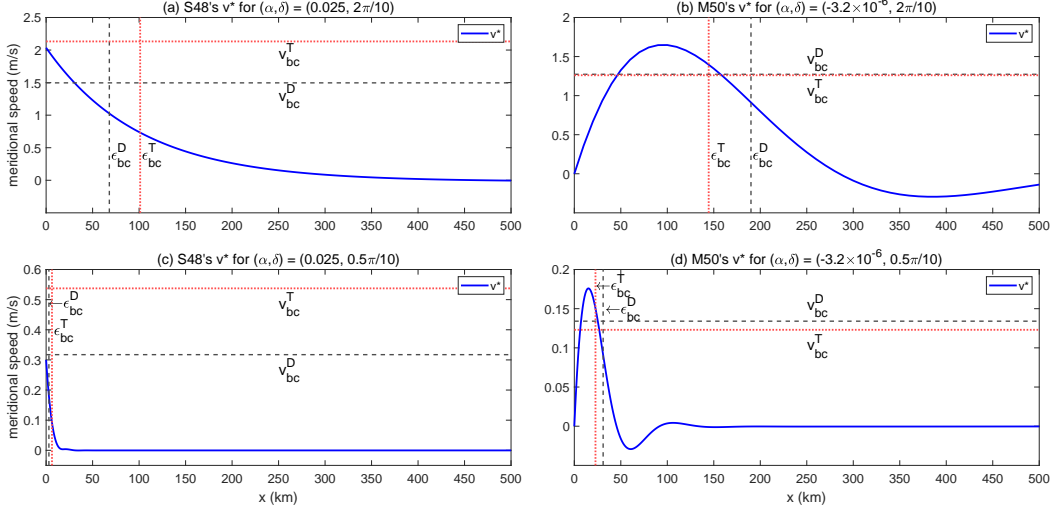
Figure 4. The meridional velocity along $y = \frac{L_y}{2}$ $\left[v^*\left(x, y = \frac{L_y}{2}\right)\right]$ in (a) S48's model for $(\alpha, \delta) = (0.025, 2\pi/10)$ and (b) M50's model for $(\alpha, \delta) = (-3 \times 10^{-6}, 2\pi/10)$; panels (c),(d) are same as (a),(b) but with $\delta = 0.5\pi/10$. The dashed black lines mark the diagnostics for the width (ϵ_{bc}^D) and the speed (v_{bc}^D) of the WBC. The dotted red lines mark the analytical estimate (proxy), $\epsilon_{bc}^T = \epsilon_{bc} L_x$, of the width and the speed, $v_{bc}^T = v_{bc}\gamma\beta L_y^2$, of the WBC. The expressions for ϵ_{bc} and v_{bc} are given by (6) [(12)] and (7) [(13)] respectively for S48's [M50's] model. For each simulation discussed here, the forcing and zonal extent of the basin are set to $\gamma = 5 \times 10^{-5}$ and $L_x = 10000$ km respectively.

of α and δ are noted above these panels) while Figure3(b),(d) depicts the steady state ψ^* obtained for parameters relevant to M50's model (and here, too, the corresponding values of α and δ are noted above these panels). The reader should note that the meridional extent (L_y) of the basin in Figure 3(a),(b) is $2\pi \times 1000$ km, whereas in Figure 3(c),(d) $L_y = \pi/2 \times 1000$ km. In all four cases the shape of the stream function is very similar to the non-dimensional stream functions (ψ) shown in Figure 1(a),(b). Moreover, for the given values of (α, δ), the ψ^*s obtained by multiplying the corresponding $\gamma\beta L_y^3$ with ψ [given by (3) for S48's model and (10) for M50's model] agree very well with the stream functions shown in Figure 3.

To benchmark our analytical expressions of the width (ϵ_{bc}) and speed (v_{bc}) of the WBC against the values obtained by the numerical simulations, we propose the following (somewhat) arbitrary diagnostics:

a) The width of the WBC (ϵ_{bc}^D) is defined as the largest value of x for which $v^*\left(x, y = \frac{L_y}{2}\right)$ [the meridional velocity along $y = \frac{L_y}{2}$] reaches half its maximum value; and

b) The speed of the WBC (v_{bc}^D) is defined as the mean of $v^*\left(x, y = \frac{L_y}{2}\right)$ between 0 and ϵ_{bc}^D.

Figure 4(a),(c) shows $v^*\left(x, y = \frac{L_y}{2}\right)$ obtained from simulations carried out for two different sets of dimensional parameters in S48's model. The dimensional parameters are chosen such that the value of $\alpha = r\frac{L_x}{\beta L_y^2} = 0.025$ is the same in the two simulations. In contrast, the value of $\delta = \frac{L_y}{L_x}$ reduces by a factor of 4 between the two simulations. Figure

309 4(b),(d) are the same as Figure 4(a),(c) except that $v^* \left(x, y = \frac{L_y}{2} \right)$ depicted is obtained from
310 simulations carried out for two different sets of dimensional parameters in M50's model. In
311 these two cases as well, the dimensional parameters are chosen to ensure that $\alpha = -\mu \frac{L_x}{\beta L_y^4} =$
312 -3.2×10^{-6} is the same while the value of δ reduces by a factor of 4 between the two
313 simulations.

314 As is evident from Figure 4(a),(c), the width of the WBC reduces from ~ 80 km to ~ 5
315 km when δ reduces from $\frac{2\pi}{10}$ to $\frac{0.5\pi}{10}$. This reduction in the width by a factor of 16 when δ is
316 decreased by a factor of 4 is consistent with (6) which shows that $\epsilon_{bc} \propto \delta^2$ in S48's model.
317 Similarly, Figure4(b),(d) show that the width of the WBC reduces from ~ 150 km to ~ 25
318 km when δ reduces from $\frac{2\pi}{10}$ to $\frac{0.5\pi}{10}$ in simulations based on M50's model. This reduction in
319 the width by a factor of 6 when δ is reduced by a factor of 4 is consistent with (12) which
320 shows that $\epsilon_{bc} \propto \delta^{\frac{4}{3}}$ in M50's model.

321 In all four cases shown in Figure 4, the differences between analytical estimate for the
322 width and speed of the WBC (denoted by ϵ_{bc}^T and v_{bc}^T) and their corresponding diagnostics
323 (denoted by ϵ_{bc}^D and v_{bc}^D) is less than a factor of 2. The agreement between our analytical
324 obtained proxies and the proposed diagnostics for the width and the speed of the WBC
325 further substantiates our findings, the implications of which are discussed in the next section.

4 Discussion and Summary

327 Since the introduction of the S48's and M50's models about 70 years ago, numerous
328 theoretical and numerical investigations have been carried out to further explore the char-
329 acteristics of westward intensification (Stommel, 1958; Hogg & Johns, 1995; Pedlosky, 2013;
330 Vallis, 2017). Both S48's and M50's dimensional models clearly bring out the contribution
331 of each source of vorticity: damping, planetary gradient and wind forcing in producing the
332 characteristic east-west asymmetry of the flow in a basin. However, the precise contribution
333 of each of the five dimensional parameters corresponding to the models i.e. L_x, L_y, β, τ_0 and
334 r/μ has only been partially analyzed or explained. In particular the effect of the domain
335 aspect ratio $\delta = \frac{L_y}{L_x}$ has received no attention in the past 70 years.

336 The formulation of S48's and M50's models in Vallis (2017) clearly highlights the effect
337 of changes in r/μ and β on the characteristics of the WBC but this formulation assumes a
338 square shaped basin and thus cannot be used to explored the effect that the basin's aspect
339 ratio has on the WBC. The role of the basin aspect ratio is the focus of the present work
340 and our analysis is based on the formulation of the non-dimensional parameter $\delta = \frac{L_y}{L_x}$ as
341 one of the two parameters in the properly scaled non-dimensional model.

342 The results of the analysis developed here, demonstrate that in both S48's and M50's
343 models, the width, speed and transport of the WBC each varies as a power law in δ for
344 sufficiently small damping — $\alpha \leq O(1)$ in S48's model and $|\alpha| \leq O(10^{-3})$ in M50's model.
345 The exponents of width, speed and transport of the WBC are 2, -1 and 1 respectively in
346 S48's model; and $\frac{4}{3}$ $-\frac{1}{3}$ and 1 respectively in M50's model. A surprising and novel result of
347 our analysis is that to first order the transport of the WBC in both models is linear with δ.
348 For typical values of damping ($\alpha = 0.02$ in S48's and $\alpha = -3 \times 10^{-6}$ in M50's model), forcing
349 ($\gamma = 5 \times 10^{-5}$), $L_x = 10000$ km and $\delta = \frac{2\pi}{10}$, the estimated non-dimensional transport is
350 0.55 in S48's and 0.48 in M50's model. The non-dimensional transport for identical values
351 of α, γ and L_x as previously mentioned, but with $\delta = 0.25$, drops to 0.14 in S48's and 0.12
352 in M50's model. This linear dependence of the non-dimensional transport on the domain
353 aspect ratio has not been quantified before and our study offers a clear appreciation of the
354 role of δ in the S48's and M50's models of westward intensification.

355 Another feature which emphasizes the treatment of δ as an important non-dimensional
356 parameter for westward intensification comes out of the proxy for the width of the WBC
357 in the two models [given by (6) and (12)]. We note that in S48's model the proxy of the

WBC's width $\sim \alpha\delta^2$ while in M50's model the same proxy $\sim (-\alpha\delta^4)^{\frac{1}{3}}$. Thus, for a constant α, a decrease in δ by a factor of 4 reduces the width of the WBC by a factor of $4^2 = 16$ in S48's model and by a factor of $4^{\frac{4}{3}} = 6$ in M50's model — this analytic result is verified by the numerical simulations described in Section 3.2. Aside from confirming our findings, the agreement between the analytically calculated proxies of the width and speed of the WBC and the diagnostics of the same proposed for the numerical simulation validates that our steady state analysis is relevant to the time-dependent dynamics of the linearized system of SWEs describing the wind-driven circulation of a barotropic ocean.

It is the proxies of width, speed and transport proposed in this study that enabled us to examine the intricate interplay between damping and domain aspect ratio in the westward intensification of wind-driven surface ocean currents. In particular, the dependence of transport of the WBC on the domain aspect ratio of the basin highlighted in this study cannot be determined using other scale analyses employed in theoretical physical oceanography. Similar proxies can also be developed in other ocean circulation models to better quantify the precise role played by a particular parameter in explaining a given phenomenon.

5 Acknowledgment

6 Data Availability Statement

The research presented in this paper is theoretical — data were not used, nor created for this research.

References

Gildor, H., Paldor, N., & Ben-Shushan, S. (2016). Numerical simulation of harmonic, and trapped, rossby waves in a channel on the midlatitude β-plane. *Quarterly Journal of the Royal Meteorological Society*, *142*(699), 2292–2299.

Hogg, N. G., & Johns, W. E. (1995). Western boundary currents. *Reviews of Geophysics*, *33*(S2), 1311–1334.

Kunzig, R. (1999). *The restless sea: exploring the world beneath the waves*. WW Norton & Company.

Munk, W. H. (1950). On the wind-driven ocean circulation. *Journal of meteorology*, *7*(2), 80–93.

Munk, W. H., & Carrier, G. F. (1950). The wind-driven circulation in ocean basins of various shapes. *Tellus*, *2*(3), 158–167.

Pedlosky, J. (2013). *Geophysical fluid dynamics*. Springer Science & Business Media.

Shamir, O., Yacoby, I., Ziskin Ziv, S., & Paldor, N. (2019). The matsuno baroclinic wave test case. *Geoscientific Model Development*, *12*(6).

Stommel, H. (1948). The westward intensification of wind-driven ocean currents. *Eos, Transactions American Geophysical Union*, *29*(2), 202–206.

Stommel, H. (1958). *The gulf stream: a physical and dynamical description*. Univ of California Press.

Sverdrup, H. U. (1947). Wind-driven currents in a baroclinic ocean; with application to the equatorial currents of the eastern pacific. *Proceedings of the National Academy of Sciences of the United States of America*, *33*(11), 318.

Vallis, G. K. (2017). *Atmospheric and oceanic fluid dynamics*. Cambridge University Press.

Veronis, G. (1966a). Wind-driven ocean circulation—part 1. linear theory and perturbation analysis. In *Deep sea research and oceanographic abstracts* (Vol. 13, pp. 17–29).

Veronis, G. (1966b). Wind-driven ocean circulation—part 2. numerical solutions of the non-linear problem. In *Deep sea research and oceanographic abstracts* (Vol. 13, pp.

406   31–55).